The Cryosphere Discuss., 5, 3291–3321, 2011
www.the-cryosphere-discuss.net/5/3291/2011/
doi:10.5194/tcd-5-3291-2011

The Cryosphere Discussions

Seasonal variations of glacier dynamics at Kronebreen, Svalbard revealed by calving related seismicity

A. Köhler[1], A. Chapuis[2], C. Nuth[1], J. Kohler[3], and C. Weidle[4]

[1]Department of Geosciences, University of Oslo, Norway
[2]Department of Mathematical Sciences and Technology, Norwegian University of Life Sciences, Norway
[3]Norwegian Polar Institute, Tromsø, Norway
[4]Department of Geosciences, Christian-Albrechts-Universität zu Kiel, Germany

Received: 21 October 2011 – Accepted: 13 November 2011 – Published: 2 December 2011

Correspondence to: A. Köhler (andreas.kohler@geo.uio.no)

Published by Copernicus Publications on behalf of the European Geosciences Union.

Abstract

We detect and cluster waveforms of seismic signals recorded close to the calving front of Kronebreen, Svalbard, to identify glacier-induced seismic events and to investigate their relation to calving processes. Single-channel geophone data recorded over several months in 2009 and 2010 are combined with eleven days of direct visual observations of the glacier front. We apply a processing scheme which combines conventional seismic event detection using a sensitive trigger algorithm and unsupervised clustering of all detected signals based on their waveform characteristics by means of Self-Organizing Maps (SOMs). We are able to distinguish between false detections, instrumental artifacts, and three classes of signals which are, with different degrees of uncertainty, emitted by calving activity. About 10 % of the directly observed calving events close to the geophone (< 1 km) can be correlated with seismic detections. By extrapolating the interpretation of seismic event classes beyond the time period of visual observations, the temporal distribution of glacier-related events shows an increase in event rate in autumn, particularly for the class which is clearly related to iceberg calving. Using the seismic event distribution in this class as a proxy for the calving rate and measurements of glacier velocity and glacier front position, we discuss the relationship between glacier dynamics and calving processes. On the seasonal time-scale, the well-marked glacier acceleration in spring is not accompanied by an increase in calving related seismicity. With a slowdown in glacier velocity in autumn, however, a remarkable increase in calving related seismicity is observed. The rate of seismic events due to calving seems thus to behave rather independently from the actual glacier speed, suggesting a complex and indirect dynamical link between the two quantities.

TCD
5, 3291–3321, 2011

1 Introduction

Iceberg calving is a key process of glacier dynamics. It is responsible for 70 % of the annual transfer of mass from glaciers to oceans (van der Veen, 1997), hence contributing to sea level rise (Nick et al., 2009). With tidewater glaciers all around the world retreating, thinning, and accelerating, it is crucial to understand the relationship between glacier dynamics and calving processes.

Iceberg calving is sporadic and therefore requires analysis of single-event data. A wide range of techniques has been used to obtain data of single-event iceberg calving including time-lapse photography (Ahn and Box, 2010), ground based radar (Chapuis et al., 2010), and seismic/acoustic monitoring (Richardson et al., 2010). However, none provide inclusive information about the size, timing, type and location of iceberg calving events, in addition to being fully automatic. So far human-based perception has been used for various glaciers (e.g., Washburn, 1936; Warren et al., 1995; O'Neel et al., 2003, 2007) and is recognized as the most practical method to acquire information about the calving processes (van der Veen, 1997). However, this technique is practically limited to short observation periods due to the very intensive work in the field. It also contains some obvious problems related to lack of attention from the observers or limited visibility due to darkness or bad weather conditions that may reduce data quality.

Seismic recordings have been used to monitor dynamic glacial activity for about 30 or 40 yr (Vanwormer and Berg, 1973; Weaver and Malone, 1979; Wolf and Davies, 1986). Studies suggest different processes generating glacier-seismic events, such as sliding at the base due to the glacial flow (Anandakrishnan and Bentley, 1993; Stuart et al., 2005), opening of cracks or crevasses (Blankenship et al., 1987; Deichmann et al., 2000), and calving (Qamar, 1988; O'Neel et al., 2007). Calving events are described as emergent, low-frequency seismic signals, and impulsive, high-frequency acoustic arrivals when measured close to the glacier front (Richardson et al., 2010). The source mechanisms can be fracture processes before the calving (O'Neel and Pfeffer, 2007)

TCD
5, 3291–3321, 2011

or the detachment itself, followed by overturning and scraping of icebergs on the ocean seafloor (Amundson et al., 2008). Most studies recorded low-magnitude glacier events at local or regional distances, though moderate glacier earthquakes have been observed globally, for example, deriving from the outlet glaciers on Greenland and in Antarctica (Ekström et al., 2003; Nettles and Ekström, 2010).

The use of seismic data supplementary to direct (visual) monitoring of calving activity therefore opens the potential to match calving activity to seismicity and thus monitor calving autonomously. Once the relation and scaling between calving events and their seismic signals is understood, seismic records may improve the understanding of glacier calving and reveal variations in calving activity over longer time periods than monitoring through direct observations.

The objectives of this study is to obtain a continuous record of calving activity over several months from seismic data recorded at Kronebreen (78′53° N, 12′30° E), a grounded, polythermal tidewater glacier, located approximately 14 km south-east of Ny-Ålesund in Western Spitsbergen (Fig. 1). Kronebreen is one of the fastest tidewater glaciers in Svalbard with an average front velocity ranging between 1 and 3.5 m per day during the summer months (Kääb et al., 2005; Rolstad and Norland, 2009) and with a terminal ice cliff having an elevation ranging from 5 to 60 m above the fjord surface at the end of August 2008 (Chapuis et al., 2010). We installed a geophone in the vicinity of the calving front from spring to autumn in 2009 and 2010 and collected ground-truth data of iceberg calving for 16 days by visual observations with an overlap of dataset of 11 days. Seismic detections are calibrated against the direct observations to extrapolate seismic signals due to calving activity beyond the ground-truth period, providing a proxy for the calving rate. In addition, we monitored the glacier velocity by using GPS measurements close to the front, and recorded the changes in front position by tracking the glacier terminus using terrestrial photogrammetry. In combination with the estimated calving rate, this data set provides an insight into glacier dynamics at the front for several months.

TCD
5, 3291–3321, 2011

2 Data

2.1 Seismic record

Several months of single-channel (vertical component) seismic data have been recorded on a PE-3 geophone from 29 June to 15 August 2009, 11 September to 11 November 2009, and 8 May to 6 November 2010 with a sampling rate of 50 Hz. A Campell CR1000 data logger recorded the raw voltage signal from the geophone which was sent to final storage through a serial cable to an Acumen compact flash memory module (because the Campbell data storage would not allow a full summer recording). This approach was restricted by transfer speed from the Campbell to the memory module which limited the amount of data we could record to 50 Hz rather than the ideal 100 Hz that is capable from the Campbell. Power supply was provided by a 12 V battery and a solar panel. In May of 2009 and 2010, the geophone was drilled 6 m into the ice and frozen into place. Melting during summer decreased the thickness of the overlaying ice layer to about 3 m. The position of the geophone (see Fig. 1), and therefore also the coupling with the ice and the noise level, differ slightly between 2009 and 2010 since the instrument has been removed during the winter months. The analysis of the seismic record in this paper does not include localization of events and the detailed investigation on their source mechanisms, as that would require more receivers, records of all three spatial wavefield components, and a sensitivity towards lower frequencies (< 10 Hz).

2.2 Direct calving observations

We monitored the calving activity at Kronebreen based on human perception (viewing and hearing). Midnight sun in this region lasts from 18 April to 24 August which allowed continuous visual monitoring of the calving activity within our summer field excursions. Four persons observed the calving front of Kronebreen during a total of 16 days split into two periods: from 14 August 2009 00:00 to 26 August 2009 16:00 GMT and from 5 August 2010 23:30 to 15 August 2010 16:00. An overlap with seismic data of

TCD
5, 3291–3321, 2011

~1.5 days in 2009 (477 observations) and 10 days in 2010 (2413 observations) are available for matching calving events to seismic detections. The camp from which we observed the glacier front was located approximately 1.5 km west of the front, which provided good coverage of the front. We estimated that 90 % of the front was visible for the observers (see Fig. 1).

For each calving event within the period of visual observation we registered the time (to a relative accuracy of 10 s), style, location and size. The style of iceberg characterizes the type of calving event. We follow O'Neel et al. (2003) classification into 6 classes: avalanches, block slumps, column drops, column rotations, submarine and internal. Avalanches and block slumps affect only parts of the glacier front, block slumps being bigger than avalanches. Column drops affect the entire subaerial part of the ice front which collapses vertically. Column rotations collapse with a rotation movement and can affect the subaerial part of the ice front alone or the entire ice wall, submarine part included. Submarine events are icebergs being detached from the ice front below the water line. The last type of event is internal and refers to either very small calving events that we could not visually observe or ice blocks falling into crevasses. In both cases they are related to glacial activity close to the front.

We also visually estimated a size for each event, which reflects the volume of ice detached from the front during a calving event. It allows a semi-quantitative approach as first introduced by Warren et al. (1995). The size scale repeats the one defined by O'Neel et al. (2003) but we extended it from 1 to 20, 20 being the entire front width collapsing. We estimated the error on the size scale caused by the subjectivity of the observers to be ±1 based on common observation periods where we compared the size each observer gave for a set of training events. This size scale is an indirect measure of iceberg volume (Chapuis and Tetzlaff, 2011).

Finally, we located each event by dividing the 3.5 km glacier front into 6 zones. Zone 6 comprises 700 m of the northernmost part of the glacier front, Zone 5 ranges from 700 to 1500 m, and Zone 1 to 4 are 500 m long each, where Zone 1 is the closest to the observation site (Fig. 1).

TCD
5, 3291–3321, 2011

2.3 Glacier velocity from GPS measurements

Glacier velocity is measured using a single code based GPS receiver approximately ~2 km from the front position. The instrument is an IMAU construction (den Ouden et al., 2010) that records one measurement every hour which is sent through ARGOS to the base server. Velocity is determined through a variety of filtering techniques based upon the number of days of smoothing. Here, we use an average of 3 days.

2.4 Front position from terrestrial photogrammetry

Repeat photographs were taken automatically every hour from the same location (star in Fig. 1) using Harbotronics time-lapse cameras (e.g., Chapuis et al., 2010). Weekly pictures are used to track the front position. Results are provided in relative changes that allow us to determine whether the glacier front was retreating or advancing, which is the most relevant information for this study. We have photographs from 9 May 2009 until 29 September 2009 and from 16 April 2010 until 13 November 2010. Details on the acquisition systems and methods are described in Chapuis et al. (2010).

3 Method

Conventional automatic event detection in seismology is usually done using Short Time Average over Long Time Average (STA/LTA) trigger algorithms which report distinct signal arrivals when amplitudes exceed the background noise level, but generally do not distinguish between different kind of events. In order to achieve a more precise classification and to handle the large amount of available data, making use of automatic pattern recognition techniques is therefore becoming increasingly important in seismological studies. Supervised classification algorithms can be employed to detect seismic events based on manually prepared training data sets (e.g., Joswig, 1990; Dowla et al., 1990). On the other hand, unsupervised pattern recognition may be used to generate

TCD
5, 3291–3321, 2011

an initial understanding of the unknown data properties without utilizing existing class or event labels as done for supervised learning (Bardainne et al., 2006; Köhler et al., 2009). Clustering is a well-known unsupervised learning method which describes the task to find a meaningful grouping of unlabeled data into respective categories (e.g., Jain, 2010). Here, we present and apply a processing scheme to detect and identify glacier-seismic signals which combines event detection using a STA/LTA trigger and clustering. While the trigger algorithm will automaticly detect all sorts of seismic events in the data, clustering detections into groups with similar signal characteristics helps to distinguish different types of seismic events and false alarms. This approach is suitable and reasonable for our purpose, since no detailed information about the character of potentially observable glacier-seismic signals was available a priori.

3.1 Seismic event detection

We use a modified version of the STA/LTA trigger function introduced by Allen (1978) which also provides an estimate for the end time of the event (STA function falls below a certain threshold for a defined number of time steps). We calibrate the algorithm parameters based on visual assessment of identified events in selected time windows. A STA window length of 0.4 s, a LTA window length of 3.5 s, and a STA/LTA threshold of 3 are chosen (other parameters: C2 = 3, C8 = 3, D8 = 1 s, D5 = 0.6 s, see Allen, 1978). This parameter setting makes the detection algorithm very sensitive to catch all event types, including short and weak ones. A drawback of such sensitivity is that the algorithm results in many false detections. We deal with this problem in the second phase of our approach.

3.2 Seismic event clustering

Although clustering is considered an unsupervised process (i.e. grouping of data itself is fully automatic), human interaction is an integral part. Choosing a meaningful number of clusters, validating and interpreting the results are crucial steps which must be

TCD
5, 3291–3321, 2011

accomplished by the analyst. Most algorithms generate a cluster solution for a fixed number of clusters and have, therefore, to be tested using different values. Furthermore, cluster validation requires an assessment whether the clustering solution is in fact a good representation of the natural grouping of the data set. In order to select the most meaningful solution, quantitative approaches can be used to compute a measure for the cluster validity, e.g. the Davies Bouldin index (DB, Davies and Bouldin, 1979). However, there is often not a single best solution and validity measures may not result in the most meaningful grouping. Visualization of clustering solutions, which must be useful also for multi-dimensional data, is one way to solve this problem (Vesanto and Alhoniemi, 2000). Finally, once a cluster solution has been found representing the natural grouping of the data, the meaning of clusters has to be determined based on expert knowledge, e.g. by considering examples or a generalized pattern from each cluster. Within this process, it might become necessary to choose another cluster solution or split and merge individual clusters.

We apply the Self-Organizing Map (SOM) technique, a quasi-artificial, unsupervised neural network used to intuitively visualize and cluster multidimensional data (Kohonen, 2001), which has been successfully applied for pattern recognition in seismology (Maurer et al., 1992; Musil and Plešinger, 1996; Tarvainen, 1999; Plešinger et al., 2000; Esposito et al., 2008; Köhler et al., 2010). The main property of SOMs is that data can be mapped on a two-dimensional, regular grid of usually hexagonal SOM units. This mapping is ordered and topology-preserving, meaning that close or similar data vectors in the input space are also close on the SOM. In that way one can visualize the distribution of multi-dimensional data in two dimensions, so that location of data projected on the SOM reflects the natural data grouping in the input space. As a final step, the SOM units can be grouped automatically using common clustering methods. For more details about the SOM method see Kohonen (2001). Examples and more detailed description of SOM clustering and visualization can be found e.g. in Köhler et al. (2009) and Köhler et al. (2010).

TCD
5, 3291–3321, 2011

In order to cluster a set of detected seismic events, a set of discriminative features is required for each detection which form the input data vector. We choose features that are potentially suitable to distinguish waveforms of different event types and false detections. These features are based on statistics on the seismogram amplitudes, the frequency spectrum, and temporal characteristics of an event (Fig. 2):

- *Number of Runs*: The number of runs is based on a significance test (Runs Test) for temporal randomness which evaluates whether all samples of a sequence are mutually independent (Wald and Wolfowitz, 1940; Köhler et al., 2009). A run of a time series is a sequence of adjacent samples below or above the mean, i.e. a white noise time series would have a high number of runs since the amplitude varies randomly around the mean over time. The seismogram time window considered to compute the number of runs begins 20 s before the event onset and ends 20 s after the event stopped according to the estimate made by the trigger function. The seismogram time window considered to compute the number of runs begins 20 s before the event onset and ends 20 s after the event stopped according to the estimate made by the trigger function.
- *Spectrum*: The frequency spectrum is computed from the detected signal only (no temporal context). The ratio of mean spectral amplitudes between 12 and 19 Hz and 0.5 to 25 Hz is computed to account for different frequency content of seismic signals.
- *SNR*: The Signal to Noise ratio is computed as the logarithmized ratio of the RMS (root mean square) of the event amplitudes and the RMS of the time window before the event which has the same length as the event.
- *Length*: The duration of the event in seconds is obtained from the STA/LTA trigger.
- *Standard deviation*: See skewness.

TCD
5, 3291–3321, 2011

– *Skewness*: Standard deviation and skewness are computed from the signal envelope. The same time window as for the number of runs is used. Both features are normalized with the mean of the envelope.

4 SOM training and cluster definition

The STA/LTA trigger generates 24 278 detections for the entire seismic record, including an unknown amount of false detections. We use all detections to generate the SOM input data set by computing the characteristics introduced above from each signal. The frequency distribution of each feature in Fig. 2 reveals that at least two distinguishable classes are present in the data set, since some features show a clear binomial distribution.

After the SOM is trained, it is clustered using an average linkage hierarchical clustering algorithm (Vesanto and Alhoniemi, 2000). Cluster solutions from 2 to 35 clusters are generated. The best solution is defined manually using the DB index as a guideline and evaluating the so-called unified distance matrix plot of the SOM (U-matrix, Fig. 3a) which illustrates the probability density distribution of data vectors (Vesanto and Alhoniemi, 2000). Comparison of the clustered SOM (Fig. 3b) and the U-matrix allows for the validation of clusterings. For a perfect grouping, cluster borders should appear as more reddish (less-dense) areas in the U-matrix plot in comparison to the regions inside the clusters. In other words, a cluster is a bounded, blue area on the SOM. We correct the number of clusters obtained from one good solution (low DB index) by splitting individual clusters based on the hierarchical cluster solution (grey clusters in Fig. 3b), resulting in 25 clusters.

TCD
5, 3291–3321, 2011

5 Results

5.1 Classification based on direct observations

The cluster solution in Fig. 3b represents the grouping of seismic detections in the feature space. However, in order to identify the meaning of each cluster, ground-truth data is required to match known event types to their corresponding clusters. Furthermore, we have to inspect detection examples from each cluster and decide what sort of signals is present based on seismological expertise. Due to the lack of man-made noise in the remote study area, we can assume that most detected seismic events are related to natural (e.g. glacial) activity.

First, all detected seismic signals are identified during the period of direct observations, in which 98 (2009) and 238 (2010) detections are obtained (white symbols on the SOM in Fig. 3b). We then match these seismic detections with directly observed calving events at the glacier front. We choose a 40 s long time window (±20 s from start of a detection) to find calving events which could be related to the corresponding seismic event. Table 1 presents a summary of the results for the different types, locations, and sizes of visually observed calving events.

In order to evaluate the resulting recognition rates and to exclude random matches, we apply a binomial test for statistical significance (Table 1). Results show that the matches for Zone 2, 3, 4, and 6 can be explained by a number obtained by chance assuming a significance level of 5 % for passing the test for randomness. Only results for Zone 1 and 5 cannot be explained by random matches. However, only calving observations in Zone 1, which is the closest to the geophone, are recognized as seismic events with a rate of 9 %, which is clearly higher than for the other zones. The rates are even higher when we only consider block slumps and column drops in Zone 1. For column rotations and submarine events, too few observation are present to obtain a reliable statistic. However, it seems that avalanches do not emit clear seismic signals strong enough to be recorded by the geophone. The recognition rate increases with size of the observed calving event up to 16 %. It is intuitively clear that only the closest

TCD
5, 3291–3321, 2011

and largest events are detectable, since the detection threshold is limited by the noise level in the seismic data. Even though we obviously are not able to monitor seismic emissions from the entire glacier front, we can proceed with investigating the subset which we are able to detect. We cannot exclude that we observe also events from the other zones (e.g. Zone 5), but only for Zone 1 the evidences are strong enough that we see indeed calving events in the seismic data.

The matching rates in Table 1 have been computed using all detections and are not based on specific clusters. However, we are now able to identify individual event clusters considering the detections matching with Zone 1 events. The red symbols in Fig. 3b represent the matching detections in the SOM space and are clearly confined to the lower part of the map. Hence, clusters located within that area are most likely glacier-event classes (i.e. iceberg calving). Some clusters do not include matches with direct observations, but the corresponding detections are clear seismic events. Furthermore, there are transition clusters where it is not clear whether the corresponding detection are instrument artifacts or very short and weak seismic events. Those clusters are not labeled as event clusters. To simplify the following discussion, we reduce the obtained clusters to four classes based on the percentage of matched detections (Zone 1) within a cluster (Table 2 and Fig. 3c). Those classes reflect the uncertainty of whether signals are related to the calving process as well as the character of its signal. The classes are:

- Class 1: Clear glacier-seismic events related to calving (> 30 % matched within cluster)
- Class 2: Most likely glacier-seismic events (> 5 % could be matched)
- Class 3: Maybe glacier-seismic events (no matches, but clearly no false detections)
- Class 4: No glacier-seismic event (instrument artifacts and triggered background noise fluctuations)

TCD
5, 3291–3321, 2011

Two matches with Zone 1 events (from 20 in total) are clearly identified as false detections (Class 4) which matched by chance (see Fig. 3b and Table 2), in agreement with what is expected from the significance test (Table 1). For the other locations, the fraction of Class 4 events among all matches is significantly higher, what confirms our hypothesis that these matches are produced by coincidence for the most part (6 of 10 for Zone 2, 5 of 6 for Zone 3, 6 of 11 for Zone 4, 11 of 13 for Zone 5, 4 of 4 for Zone 6).

5.2 Seismic signal characteristics

In order to investigate the meaning of clusters, SOM component plane plots are useful for displaying the feature distribution or values of a particular data vector component which is associated with any of the SOM units (Fig. 3d–f). Randomly selected examples of seismic waveforms (Fig. 4) and the SOM component planes show the different characteristics of each event class. As expected, all event clusters (Class 1 to 3) are characterized by high signal to noise ratios (SNR) compared to the rest of detections (Fig. 3f). Class 1, which is clearly related to iceberg calving, consists of rather long events, typically 4–10 s (see Fig. 3d), with several local maxima in their amplitude (Fig. 4). Very short signals seem to be characteristic of Class 2. Detections with high amplitude peaks (higher standard deviation, Fig. 3e) mainly belong to the event group which could not be correlated with calving events (Class 3).

We do not observe typical seismic signals with clearly separated P and S-Wave onsets. The complexity of waveforms, especially those of Class 1 (Fig. 4), could reflect the nature of a calving event, which is rather a sequence of events than a signal from a single, shortly acting source. It is also possible that we observe parts of the acoustic signal of an event coupled with the ice surface in addition to direct seismic waves (Richardson et al., 2010). It should be noted that due to the limited sensitivity of the instrument we are not able to record seismic signals at longer periods which have been shown to be emitted by calving events (Richardson et al., 2010).

TCD
5, 3291–3321, 2011

5.3 Temporal patterns in glacier-related seismicity

We obtain 138 detections belonging to Class 1, 2, and 3 which can be interpreted as glacier-seismic events within the period of direct observation. When we assume that seismic signals are generated by the same (glacial) processes over the year, a number of 7850 events occurred within the entire time of seismic measurement, among which 792 belong to Class 1. Seismic activity seems to be generally higher in 2009 compared to 2010 (Fig. 5). However, the comparison between the absolute event rates in both years might be biased due to changing location and coupling of the instrument. In both years the event activity seems to be higher in autumn than in the summer months.

The general seasonal trend is overlaid by short-term patterns of periods of 10 to 15 days in both years. For Class 1 events several peaks in the event rate in July 2009 are observed. However, at least one minimum of activity in July coincides with increase background noise level in the seismic data (see Fig. 5a). Therefore, it is not clear whether simply less events are detected on the geophone or less signals are emitted by the glacier. In 2010, the noise level is more stable besides one peak in the beginning of May. The noise level seems to increase slightly in summer 2010 which could be a result of decreasing burial depth of the geophone or continuous emitted noise of melt water. There are pronounced peaks in event rate in May and in beginning of August for Class 1 events (Fig. 5b).

5.4 Extrapolation of calving rate beyond calibration period

Within the time period of direct observations, Class 1 is clearly related to iceberg calving. We have to make two assumptions if we want to extrapolate the event rate of this class as a proxy for the calving rate beyond the calibration period. First, there should be no other dominant process at the glacier that generates Class 1 events in the calibration period and behaves independently from calving over time (e.g. basal sliding, fracturing). We have to consider this possibility since about 43 % of the Class 1 events do not exhibit matches with directly observed calving (Table 2). Secondly, even if all

TCD
5, 3291–3321, 2011

Class 1 events are generated by calving in the calibration period, there could be another process which is not active in the calibration period and generates Class 1 events at another time. However, different glacial processes have been shown to emit signals with different characteristics (e.g., Stuart et al., 2005; West et al., 2010). Therefore, the clustering which we performed should be able to distinguish those processes. Furthermore, when we assess similarity of seismic events on a more detailed level and consider sub-clusters of Class 1, i.e. divide the class into the hexagonal SOM units (see Fig. 3) and consider the associated seismic detection, we observe the same temporal patterns as for all events in Class 1 and no sub-cluster includes events which occur within particular time periods only. Therefore, we have good indications that most events in Class 1 are indeed related to calving, however we cannot fully exclude the possibility that other processes or local seismic sources could be entrapped in our proxy for glacier calving due to the limitations of our data set. Note that Class 1 events do not represent the total amount of calving events at the entire glacier front, but consist of signals emitted by the largest events close to the measurement site.

5.5 Relationship between calving process and glacier dynamics

Recent thinning, acceleration and retreat of tidewater in different parts of the world raises the question of the relationship between calving processes and glacier dynamics. Is iceberg calving the cause or the consequence of glacier acceleration? Benn et al. (2007) reported that an equal number of studies bring evidence in favor for both views, calving causing glacier flow increase (e.g., Hughes, 1986; Motyka et al., 2003; Joughin et al., 2004; Nick et al., 2009) and increased calving activity following glacier acceleration (e.g., Venteris et al., 1997; Kirkbride and Warren, 1999).

To investigate the relationship between glacier speed and calving activity on seasonal time-scales, we analyzed qualitatively the three dataset available for 2009 and 2010: indirect measurement of iceberg calving (counts from seismic monitoring), glacier velocity (GPS measurements) and front positions (photogrammetry). In Fig. 5 the front position is indicated by a relative position compared to the first day

TCD
5, 3291–3321, 2011

of observations. Furthermore, the change in front position is shown (first derivative). A positive front position indicates advance and negative retreat of the front with respect to the reference date. The solid green line represents the average position of the entire front while the dashed green line represents the front position only in Zone 1. We attempt to generate a timeline of the processes described above to determine which happened first and triggered the other ones.

For the year 2009 (Fig. 5a), the glacier speed is rather constant during the spring with acceleration beginning in mid-June, several peaks during the summer and deceleration at the end of July. Velocity remains more or less constant during the entire autumn except a peak at the end of August caused by a rather large rain event. The calving related seismicity, represented by the seismic Class 1 events, remains rather low during the summer with three peaks that are more or less synchronous with the glacier speed peaks. During the autumn, our proxy for calving activity is about three times larger than during the summer. Finally, the glacier front slowly advances during the spring, reaching a plateau at the beginning of July when the front advance is at its maximum. The front remains rather constant all summer and starts retreating at the mid to end of July until the end of September (end of our photographs dataset). The change in front position is positive only during spring, it then becomes zero until the beginning of July and then negative until the end of September.

In 2010 (Fig. 5b), the glacier speed starts to increase in mid-May until a maximum is reach at the end of June, followed by a short decrease and another maximum at the end of July before decreasing drastically until mid-August where it reaches another smaller maximum and finally decreases until the end of September. The calving related seismicity remains rather low during the spring and the summer apart for two maxima, one mid-May and one at the beginning of August. The last one correlates well with an increase in velocity. At the end of August the calving related seismicity is increasing and staying at a higher level than during summer until the end of October. Finally the glacier position behaves differently than in 2009 with a fast and constant advance from mid-April until mid or the end of July, immediately followed by a rather fast and

TCD
5, 3291–3321, 2011

constant retreat until the beginning of October when it starts to plateau while continuing to retreat. The change in front position is mostly positive until mid-July, is zero for a few weeks and then becomes negative until mid-November.

From the two reconstructed timelines we can identify some patterns in the timing of the glacier dynamic events. Seismicity as a proxy for iceberg calving remains relatively low from May until mid-September while both velocity and front position undergo large fluctuations. For both years, calving related seismicity increases in the autumn, when velocity is lowest and rather constant and the front retreating. Changes in velocity do not affect the seasonal fluctuations observed in calving related seismicity, namely low activity during spring and summer and increased activity from September on. On the other hand, changes in velocity might affect small, weekly variations observed in calving related seismicity, with an increase of iceberg discharge when velocity increases, as in the case in spring 2009 and early August 2010.

On seasonal time-scales, calving seems to be a dynamical process not following the variation in velocity. Calving related seismicity shows marked increase in the autumn, which is visually translated by a continuous retreat of the glacier front. In this case, the large release of ice at the front cannot be explained by a larger ice flux, since velocity is at its lowest and rather constant. This shows that our proxy for the calving rate is controlled by other dynamical variables and that calving activity seems not to be directly related to the absolute value of glacier velocity at the front. Velocity and calving related seismicity are obviously linked, but through intermediate processes like stretching rate that favors the opening of crevasses (Venteris et al., 1997), basal velocity that influences the basal conditions, velocity linked to stretching of the ice and potentially thinning, etc., all those processes leading to a more unstable glacier front more prone to calving.

TCD
5, 3291–3321, 2011

6 Conclusions

We have analyzed seismic data and direct visual observations of calving events at the terminus of Kronebreen, Svalbard. We have applied a traditional STA/LTA trigger algorithm with a very sensitive setting to detect seismic signals emitted by glacial activity. The signals of all detections have been clustered to distinguish between different types of events and false detections. For clustering and identification of event clusters Self-Organizing Maps have been used which simplifies visualizations of multi-dimensional data. By comparing ground-truth data from the calving front with the obtained seismic detections, we are able to match about 10 % of close calving events (< 1 km from the geophone) with seismic signals. This allows us to define three seismic event classes which are, with different degrees of uncertainty, related to glacier activity.

By extrapolating our results beyond the time of direct observations, about 5100 seismic events are detected overall during several months in 2009 and 2010, including signals due to calving and probably also signals emitted by other sources in the glacier. The class of seismic events clearly related to calving activity suggests about 790 larger calving events in the vicinity of the seismic instrument. We have found that we are not able to monitor the entire calving front and to detect smaller events due to the noise level in the seismic data. This may be a result of the low sensitivity of the geophone. Nevertheless, using this subset of events as a proxy for activity at the glacier front, temporal patterns in the event rate are found that reveal seasonal changes.

We have analyzed the relationship between glacier velocity, front position and calving rate. Higher calving related seismicity is found in autumn compared to the summer. Considering short-term variations, the seismic event rate is at least partially correlated with patterns in the ice flow velocity measured close to the glacier front with peaks in velocity corresponding to small peaks in calving related seismicity. However, on a seasonal time-scale, velocity and rate of seismic events due to calving behave rather independently: in the autumn we observe a large increase in calving related seismicity while velocity is constant and at its lowest values for the year. On seasonal time-scales,

TCD
5, 3291–3321, 2011

iceberg calving might be controlled by other glacier dynamical processes like stretching rate, basal sliding, crevasse deepening due to melt water at the glacier surface, buoyancy perturbations, front destabilization due to changes in the front geometry or to calving activity itself (Chapuis and Tetzlaff, 2011).

Our results show the capability of monitoring glacier activity with seismic receivers to extend observational data sets and to obtain new insights about glacier dynamics. We found that a single-channel geophone, although limited by its sensitivity, can deliver useful information about calving activity. Improving the autonomous classification of calving related seismicity will benefit from more than one instrument to determine the location of seismic sources at the glacier as well as more sensitive instrumentation (e.g. broadband receivers) allowing deeper investigation into the seismic characteristics of glacier induced signals.

Acknowledgements. The calving observation project was supported by the IPY-GLACIODYN project (176076) funded by the Research Council of Norway (NFR). Fieldwork was made possible thanks to the Svalbard Science Forum funding (NFR). We would also like to thank Allan Buras, Bas Altena, Karin Amby, Damien Isambert and Mari Svanem for their great work observing the glacier in the field. Special thanks go to Tobias Baumann for the implementation of the STA/LTA trigger algorithm. Figures have been generated using the SOM toolbox (Vesanto et al., 2000) and the Generic Mapping Tools (Wessel and Smith, 1998).

References

Ahn, Y. and Box, J.: Glacier velocities from time-lapse photos: technique development and first results from the Extreme Ice Survey (EIS) in Greenland, J. Glaciol., 56, 723–734, doi:10.3189/002214310793146313, 2010. 3293

Allen, R. V.: Automatic earthquake recognition and timing from single traces, B. Seismol. Soc. Am., 68, 1521–1532, 1978. 3298

Amundson, J. M., Truffer, M., Lüthi, M. P., Fahnestock, M., West, M., and Motyka, R. J.: Glacier, fjord, and seismic response to recent large calving events, Jakobshavn Isbræ, Greenland, Geophys. Res. Lett., 35, L22501, doi:10.1029/2008GL035281, 2008. 3294

TCD
5, 3291–3321, 2011

Anandakrishnan, S. and Bentley, C. R.: Micro-earthquakes beneath Ice Streams Band C, West Antarctica: observations and implications, J. Glaciol., 39, 455–462, 1993. 3293
Bardainne, T., Gaillot, P., Dubos-Sallée, N., Blanco, J., and Sénéchal, G.: Characterization of seismic waveforms and classification of seismic events using chirplet atomic decomposition. Example from the Lacq gas field (Western Pyrenees, France), Geophys. J. Int., 166, 699–718, doi:10.1111/j.1365-246X.2006.03023.x, 2006. 3298
Benn, D. I., Warren, C. R., and Mottram, R. H.: Calving processes and the dynamics of calving glaciers, Earth-Sci. Rev., 82, 143–179, doi:10.1016/j.earscirev.2007.02.002, 2007. 3306
Blankenship, D. D., Anandakrishnan, S., Kempf, J. L., and Bentley, C. R.: Microearthquakes under and alongside Ice Stream B, Antarctica, detected by a new passive seismic array, Ann. Glaciol., 9, 30–34, 1987. 3293
Chapuis, A. and Tetzlaff, T.: What do the distributions of calving-event sizes and intervals say about the stability of tidewater glaciers?, J. Glaciol., in prep., 2011. 3296, 3310
Chapuis, A., Rolstad, C., and Norland, R.: Interpretation of amplitude data from a ground-based radar in combination with terrestrial photogrammetry and visual observations for calving monitoring of Kronebreen, Svalbard, Ann. Glaciol., 51, 34–40, doi:10.3189/172756410791392781, 2010. 3293, 3294, 3297
Davies, D. L. and Bouldin, D. W.: A cluster separation measure, IEEE T. Pattern Anal., 1, 224–227, doi:10.1109/TPAMI.1979.4766909, 1979. 3299
Deichmann, N., Ansorge, J., Scherbaum, F., Aschwanden, A., Bernardi, F., and Gudmundsson, G. H.: Evidence for deep icequakes in an Alpine glacier, Ann. Glaciol., 31, 85–90, doi:10.3189/172756400781820462, 2000. 3293
Dowla, F. U., Taylor, S. R., and Anderson, R. W.: Seismic discrimination with artificial neural networks: preliminary results with regional spectral data, B. Seismol. Soc. Am., 80, 1346–1373, 1990. 3297
Ekström, G., Nettles, M., and Abers, G. A.: Glacial earthquakes, Science, 302, 622–624, doi:10.1126/science.1088057, 2003. 3294
Esposito, A. M., Giudicepietro, F., D'Auria, L., Scarpetta, S., Martini, M. G., Coltelli, M., and Marinaro, M.: Unsupervised neural analysis of very-long-period events at Stromboli volcano using the self-organizing maps, B. Seismol. Soc. Am., 98, 2449–2459, doi:10.1785/0120070110, 2008. 3299
Hughes, T.: The Jakobshanvs effect, Geophys. Res. Lett., 13, 46–48, doi:10.1029/GL013i001p00046, 1986. 3306

TCD
5, 3291–3321, 2011

Jain, A.: Data clustering: 50 years beyond K-means, Pattern Recogn. Lett., 31, 651–666, doi:10.1016/j.patrec.2009.09.011, 2010. 3298
Joswig, M.: Pattern recognition for earthquake detection, B. Seismol. Soc. Am., 80, 170–186, 1990. 3297
Joughin, I., Abdalati, W., and Fahnestock, M.: Large fluctuations in speed on Greenland's Jakobshavn Isbrae glacier., Nature, 432, 608–610, doi:10.1038/nature03130, 2004. 3306
Kääb, A., Lefauconnier, B., and Melvold, K.: Flow field of Kronebreen, Svalbard, using repeated Landsat 7 and ASTER data, Ann. Glaciol., 42, 7–13, doi:10.3189/172756405781812916, 2005. 3294
Kirkbride, M. P. and Warren, C. R.: Tasman Glacier, New Zealand: 20th-century thinning and predicted calving retreat, Global Planet. Change, 22, 11–28, doi:10.1016/S0921-8181(99)00021-1, 1999. 3306
Köhler, A., Ohrnberger, M., and Scherbaum, F.: Unsupervised feature selection and general pattern discovery using Self-Organizing Maps for gaining insights into the nature of seismic wavefields, Comput. Geosci., 35, 1757–1767, doi:10.1016/j.cageo.2009.02.004, 2009. 3298, 3299, 3300
Köhler, A., Ohrnberger, M., and Scherbaum, F.: Unsupervised pattern recognition in continuous seismic wavefield records using Self-Organizing Maps, Geophys. J. Int., 182, 1619–1630, doi:10.1111/j.1365-246X.2010.04709.x, 2010. 3299
Kohonen, T.: Self-Organizing Maps, Vol. 30 of Springer Series in Information Sciences, third extended edn., Springer, Berlin, Heidelberg, New York, 2001. 3299
Maurer, W. J., Dowla, F. U., and Jarpe, S. P.: Seismic event interpretation using self-organizing neural networks, Proceedings of the SPIE – The International Society for Optical Engineering, 1709, 950-958, doi:10.1117/12.139971, 1992. 3299
Motyka, R. J., O'Neel, S., Connor, C. L., and Echelmeyer, K. A.: Twentieth century thinning of Mendenhall Glacier, Alaska, and its relationship to climate, lake calving, and glacier run-off, Global Planet. Change, 35, 93–112, doi:10.1016/S0921-8181(02)00138-8, 2003. 3306
Musil, M. and Plešinger, A.: Discrimination between local microearthquakes and quarry blasts by multi-layer perceptrons and Kohonen maps, B. Seismol. Soc. Am., 86, 1077–1090, 1996. 3299
Nettles, M. and Ekström, G.: Glacial earthquakes in Greenland and Antarctica, Annu. Rev. Earth Pl. Sc., 38, 467–491, doi:10.1146/annurev-earth-040809-152414, 2010. 3294
Nick, F. M., Vieli, A., Howat, I. M., and Joughin, I.: Large-scale changes in Greenland outlet

TCD
5, 3291–3321, 2011

glacier dynamics triggered at the terminus, Nat. Geosci., 2, 110–114, doi:10.1038/ngeo394, 2009. 3293, 3306

O'Neel, S. and Pfeffer, W. T.: Source mechanics for monochromatic icequakes produced during iceberg calving at Columbia Glacier, AK, Geophys. Res. Lett., 34, L22 502, doi:10.1029/2007GL031370, 2007. 3293

O'Neel, S., Echelmeyer, K. A., and Motyka, R. J.: Short-term variations in calving of a tidewater glacier: LeConte Glacier, Alaska, USA, J. Glaciol., 49, 587–598, doi:10.3189/172756503781830430, 2003. 3293, 3296

O'Neel, S., Marshall, H. P., McNamara, D. E., and Pfeffer, W. T.: Seismic detection and analysis of icequakes at Columbia Glacier, Alaska, J. Geophys. Res., 112, F03S23, doi:10.1029/2006JF000595, 2007. 3293

den Ouden, M. A. G., Reijmer, C. H., Pohjola, V., van de Wal, R. S. W., Oerlemans, J., and Boot, W.: Stand-alone single-frequency GPS ice velocity observations on Nordenskildbreen, Svalbard, The Cryosphere, 4, 593–604, doi:10.5194/tc-4-593-2010, 2010. 3297

Plešinger, A., Růžek, B., and Boušková, A.: Statistical interpretation of WEBNET seismograms by artificial neural nets, Stud. Geophys. Geod., 44, 251–271, doi:10.1023/A:1022119011057, 2000. 3299

Qamar, A.: Calving icebergs: a source of low-frequency seismic signals from Columbia Glacier, Alaska, J. Geophys. Res., 93, 6615–6623, doi:10.1029/JB093iB06p06615, 1988. 3293

Richardson, J. P., Waite, G. P., FitzGerald, K. A., and Pennington, W. D.: Characteristics of seismic and acoustic signals produced by calving, Bering Glacier, Alaska, Geophys. Res. Lett., 37, L03503, doi:10.1029/2009GL041113, 2010. 3293, 3304

Rolstad, C. and Norland, R.: Ground-based interferometric radar for velocity and calving-rate measurements of the tidewater glacier at Kronebreen, Svalbard, Ann. Glaciol., 50, 47–54, doi:10.3189/172756409787769771, 2009. 3294

Stuart, G., Murray, T., Brisbourne, A., Styles, P., and Toon, S.: Seismic emissions from a surging glacier: Bakaninbreen, Svalbard, Ann. Glaciol., 42, 151–157, doi:10.3189/172756405781812538, 2005. 3293, 3306

Tarvainen, M.: Recognizing explosion sites with a self-organizing network for unsupervised learning, Phys. Earth Planet. In., 113, 143–154, doi:10.1016/S0031-9201(99)00019-9, 1999. 3299

Vanwormer, D. and Berg, E.: Seismic evidence for glacier motion, J. Glaciol., 12, 259–265, 1973. 3293

TCD
5, 3291–3321, 2011

van der Veen, C. J.: Calving Glaciers: Report of a Workshop February 28–March 2, 1997, Tech. rep., BPRC Report No. 15, Byrd Polar Research Center, The Ohio State University, Columbus, Ohio, 1997. 3293
Venteris, E. R., Whillans, I. M., and van der Veen, C. J.: Effect of extension rate on terminus position, Columbia Glacier, Alaska, USA, Ann. Glaciol., 24, 49–53, 1997. 3306, 3308
Vesanto, J. and Alhoniemi, E.: Clustering of the self-organizing map, IEEE T. Neural Networ., 11, 586–600, doi:10.1109/72.846731, 2000. 3299, 3301
Vesanto, J., Himberg, J., Alhoniemi, E., and Parhankangas, J.: SOM toolbox for Matlab, Tech. rep., Helsinki University of Technology, Helsinki, 2000. 3310
Wald, A. and Wolfowitz, J.: On a test whether two samples are from the same population, Ann. Math. Stat., 11, 147–162, doi:10.1214/aoms/1177731909, 1940. 3300
Warren, C. R., Glasser, N. F., Harrison, S., Winchester, V., Kerr, A. R., and Rivera, A.: Characteristics of tide-water calving at Glaciar San Rafael, Chile, J. Glaciol., 41, 273–289, 1995. 3293, 3296
Washburn, B.: Exploring Yukon's glacial stronghold, N. Geog. Mag., 69, 715-748, 1936. 3293
Weaver, C. S. and Malone, S. D.: Seismic evidence for discrete glacier motion at the rock-ice interface, J. Glaciol., 23, 171–184, 1979. 3293
Wessel, P. and Smith, W. H. F.: New, improved version of GMT released, EOS T. Am. Geophys. Un., 79, 579–579, doi:10.1029/98EO00426, 1998. 3310
West, M., Larsen, C., Truffer, M., O'Neel, S., and LeBlanc, L.: Glacier microseismicity, Geology, 38, 319–322, doi:10.1130/G30606.1, 2010. 3306
Wolf, L. W. and Davies, J. N.: Glacier-generated earthquakes from Prince William Sound, Alaska, B. Seismol. Soc. Am., 76, 367–379, 1986. 3293

TCD
5, 3291–3321, 2011

Table 1. Results of the matching between seismic detections and visually observed calving events for 11 days. "All" means that all observations are used including a number of 101 not assigned to one of the 6 Zones. "Matching Rate" is percentage of visual observations that can be related to seismic detections. "Significance Random Match" refers to binomial test for statistical significance of matches. It is significance that matches can be produced by chance.

Calving Events	Visual Observations	Seismic Matches	Matching Rate	Significance Random Match
All	2890	67	2.3 %	0 %
Zone 1	222	20	9.0 %	0 %
Zone 2	709	10	1.4 %	38.5 %
Zone 3	488	6	1.2 %	50.7 %
Zone 4	717	11	1.5 %	28.7 %
Zone 5	469	13	2.8 %	0.6 %
Zone 6	184	4	2.2 %	11.2 %
Zone 1 avalanches	18	0	0 %	22.1 %
Zone 1 block slumps	39	5	12.8 %	0 %
Zone 1 column drops	17	2	11.8 %	0.2 %
Zone 1 column rotations	6	1	16.7 %	0.3 %
Zone 1 submarine	2	0	0 %	2.7 %
Zone 1 internal	140	12	8.6 %	0 %
Zone 1 Size 1	148	11	7.4 %	0 %
Zone 1 Size 2	43	5	11.6 %	0 %
Zone 1 Size 3	25	4	16 %	0 %
Zone 1 Size > 3	6	0	0 %	8.0 %

TCD
5, 3291–3321, 2011

Table 2. Event classes obtained from clustering and defined based on matching seismic detections and visual observations. Class 1: clear glacier events related to calving, Class 2: most likely glacier events, Class 3: maybe glacier events, Class 4: no glacier events. "Detections in Matching period" is the number of seismic detections during the matching/ground-truth period. "Matches Zone 1" is number (and percentage) of seismic detections which can be related to a direct observation in Zone 1. "All detections" refers to seismic detection within entire time of seismic recording in 2009 and 2010. The last column states the clusters merged to define classes (see Fig. 3b,c).

Class label	Detections in Matching Period	Matches Zone 1	All Detections	Clusters
1	9	5 (56.6 %)	792	4, 16, 20
2	107	13 (12.2 %)	3699	6, 9, 10, 11
3	22	0	3359	1–3, 5, 12, 18, 19, 21, 22
4	200	2 (1 %)	16 428	7, 8, 13–15, 17, 23–25

TCD
5, 3291–3321, 2011

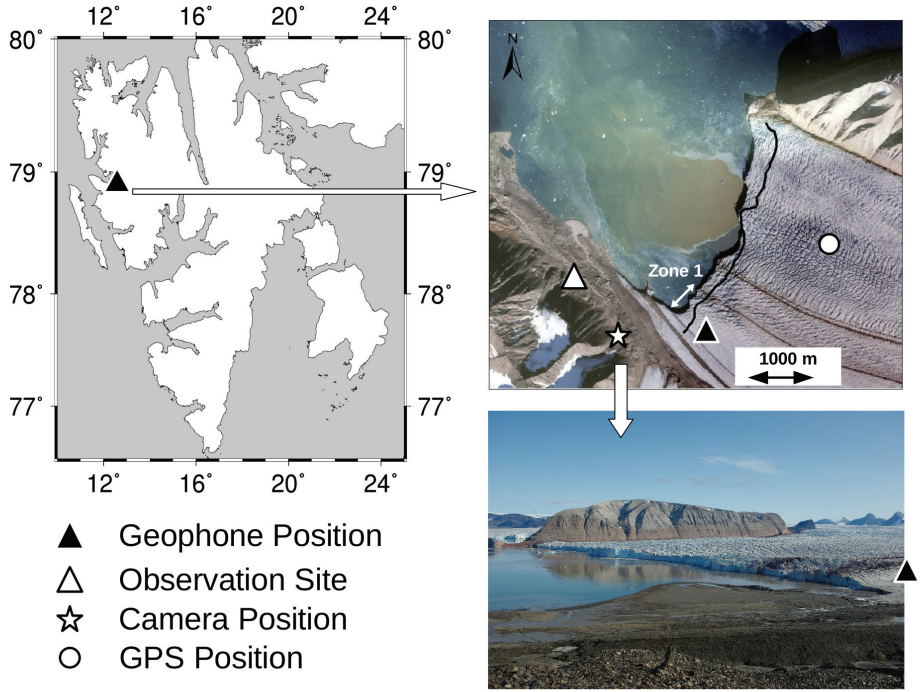

Fig. 1. Location of Kronebreen on Svalbard and position of instrumentation and observation site close to the calving front. Lower photo shows view of glacier front as seen from the camera position close to the visual observation site.

TCD
5, 3291–3321, 2011

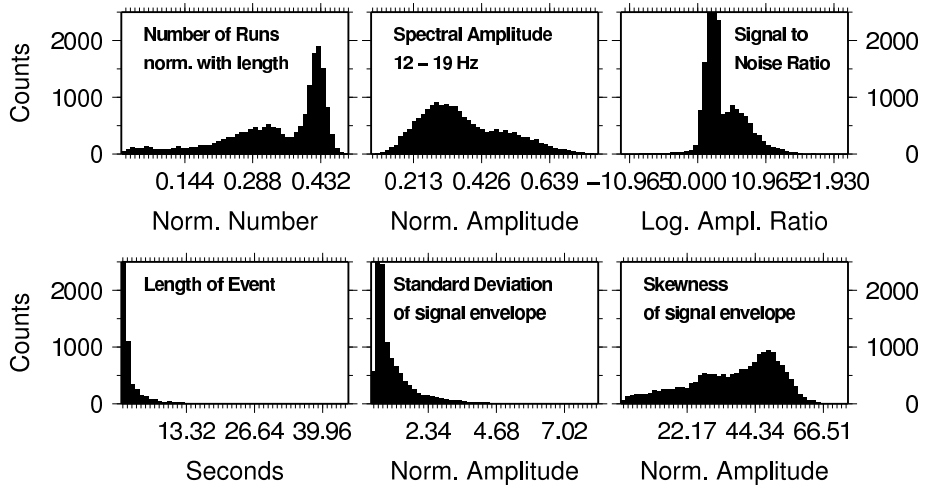

Fig. 2. Distribution of features forming the input data vector for clustering computed for all detected seismic events. A mixture of at least two normal distributions denotes existence of clusters.

TCD
5, 3291–3321, 2011

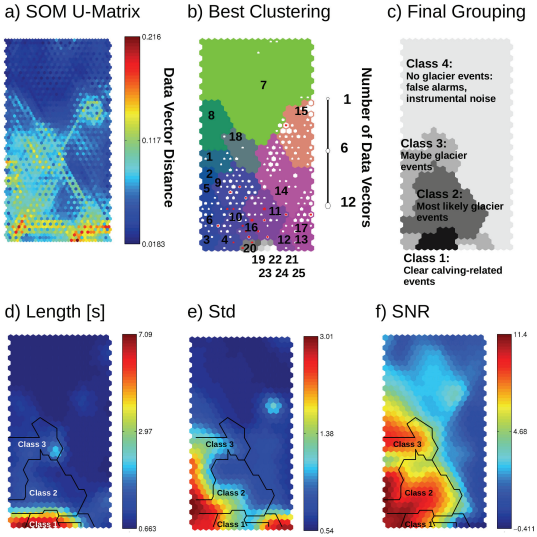

Fig. 3. SOM and clustering of detected seismic events. **(a)** Unified distance matrix (U-matrix) which reveals data density in input space. Each SOM unit is divided into seven sub-unit. Each sub-unit is colored according to distance between corresponding data vectors of neighbor units. Areas with low distances (blue) indicate high data density (i.e. clusters). **(b)** Cluster solution chosen based on U-matrix and DB index (see text). Cluster membership of each SOM unit is indicated by color. Clusters with a grey scale fill are those which are obtained by splitting clusters from one solution with 18 clusters. Symbols show data projected on the SOM. Sizes of hexagons correspond to number of projected data vectors represented by a SOM unit. White symbols correspond to detections within 11 days long period where direct observations of glacier front are available (matched and unmatched). Red symbols are the detections matching with events observed in Zone 1. **(c)** Final grouping of events based on matching rates and inspection of examples from each cluster. **(d–f)** Component planes for three selected features: Length of a detections, Standard deviation of signal envelope, and signal to noise ratio. Each SOM unit is colored according to value of a particular data vector component. Red colors stand for high values of the corresponding feature. Outline of signal classes is indicated.

TCD
5, 3291–3321, 2011

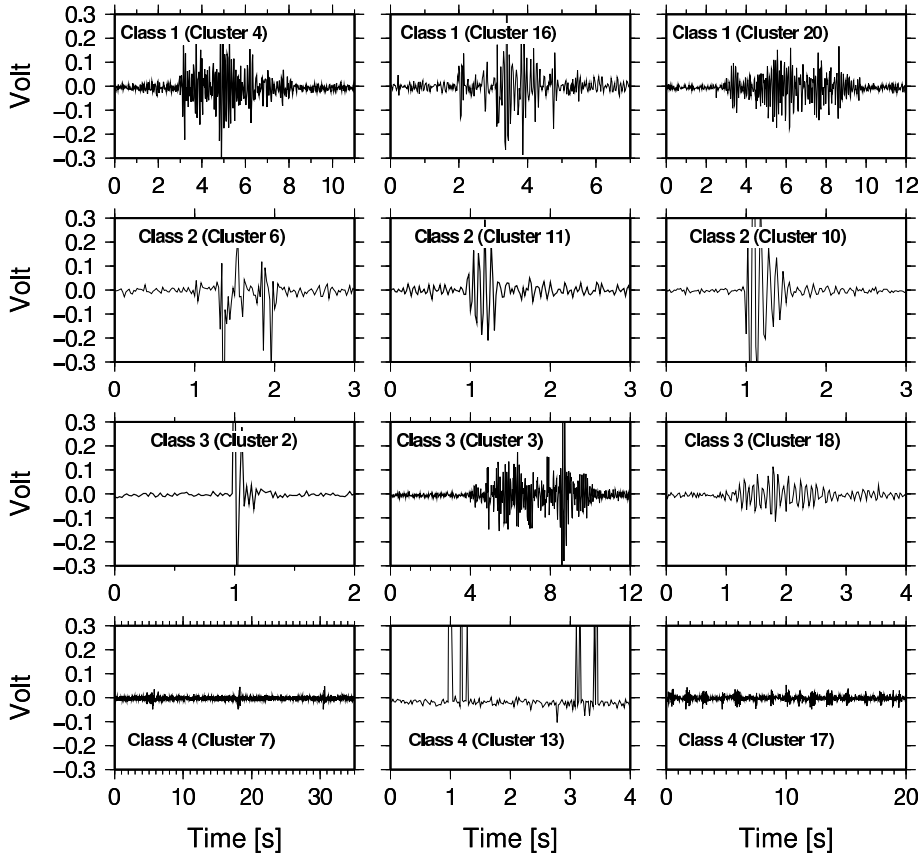

Fig. 4. Randomly selected examples of all event classes. Class 1: clear calving-related seismic events, Class 2: most likely glacier events, Class 3: maybe glacier events, Class 4: no glacier events. Same amplitude scale for all classes.

TCD
5, 3291–3321, 2011

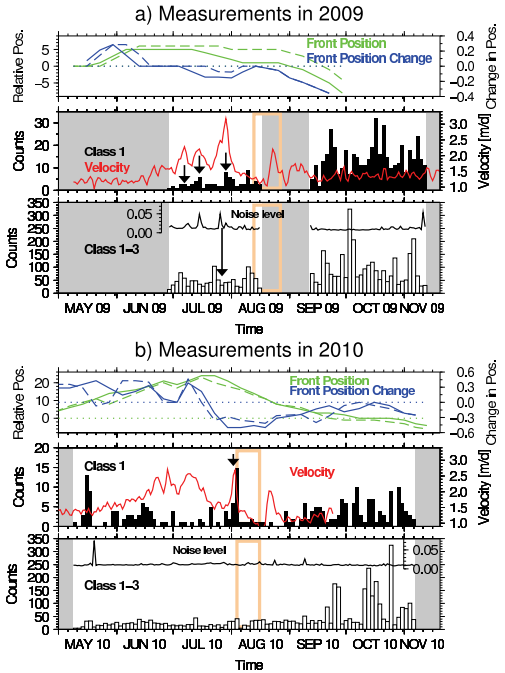

Fig. 5. Temporal distribution of seismic detections belonging to event classes 1 to 3 and Class 1 only. Class 1 are seismic events clearly related to iceberg calving. Scale for counts is different for 2009 and 2010. Noise level in seismic data is shown using same scale for amplitude as in Fig. 4. Grey areas represent data gaps and orange boxes periods of direct (visual) calving observations. Red curve shows velocity of Kronebreen measured close to the calving front. Arrows indicate short-term correlations between GPS velocity, noise level, and event rate. Green curve represents average, relative position and blue curve change in front position of the entire front. Dashed lines indicate front position and change only in Zone 1. Horizontal, green-dotted curve shows position at first day of measurement (zero) and blue-dotted curve no change in front position. Positive values correspond to advance and negative to retreat of front.

TCD
5, 3291–3321, 2011